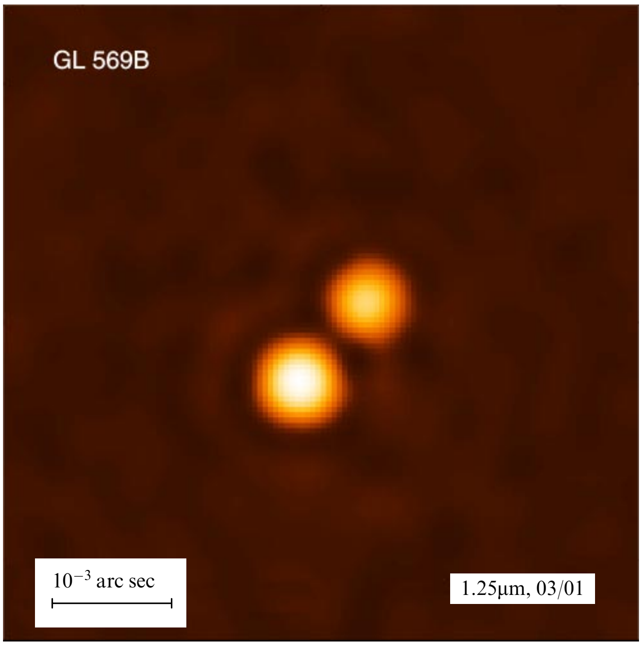

Figure 5. The image of the system of dwarfs Gl 569B obtained on the BTA telescope using IR speckle-interferometry at 1.3 μm. The distance between the components is 0.089″ (≈ 1 a.u.).

different formation mechanisms of stars and very low-mass substellar objects.

The number of BDs and the mass function. Now more than half the area of the Pleiades cluster has been searched for the presence of BDs. The BDs turn out to form a numerous population containing up to 10% of the total cluster mass. The survey of the field stars in the Northern hemisphere by the 2MASS telescope at the wavelength 2 μm, which has already revealed more than 200 new BDs, allowed astronomers to conclude that the mass function of low-mass objects has the form $dN/dM = M^{\alpha}$ with $2 > \alpha > 1$. If $\alpha \approx 1.3$, the local density of BDs with $0.075 > M/M_{\odot} > 0.01$ is about 0.1 system per pc^3, or $\sim 0.005\ M_{\odot}\ \mathrm{pc}^{-3}$. This means that BDs are as numerous as stars in the Galaxy disk, but they contribute not more than 10% of the total mass. The estimate of the number of T-dwarfs with surface temperatures below 1000 K gives the same order of magnitude. The microlensing observations of stars in the direction of the central parts of the Galaxy also suggest that BDs contribute less than 10% of the stellar mass. Therefore, substellar objects may be our most wide-spread neighbors, however the possibility that they are responsible for the dark matter in the Galaxy is totally excluded (this would require $\alpha > 3$).

Formation of BDs. There are three possible BD formation mechanisms. (a) BDs result from the collapse of a hierarchically structured protostellar cloud, like stars with larger masses. The hierarchical cloud model always produces the Salpeter mass function. Calculations show that in cold clouds ($T \sim 3$ K), up to 50% of the mass and up to 90% of the number of objects will be BDs. (b) BDs are formed as a result of gravitational instability of a gas-dust disk around a forming star. This model somewhat contradicts the small fraction of the observed BDs — companions to ordinary stars. (c) BDs originate from the ejection of stellar embryos from the star forming region due to momentum and energy exchanges. For an embryo to have no time to acquire mass, the characteristic time before the ejection must be very short, $\sim 10^3 - 10^4$ years. However, recent measurements of the BD radial velocity dispersion in the dark molecular cloud in Chameleon indicated that it does not differ from the velocities of the surrounding stars and gas and, hence, no escape velocities are observed.

Problems. The immediate problems of the BD studies include the determination of the BD cooling curves to specify the atmosphere models, the determination of the mass of individual interacting systems, the mass function specification to determine the BD contribution to the dark matter in the Galaxy. Ground-based possibilities of BD observations are very limited. New space experiments like IRIS, SIRTF, and NASA Planet Finder may discover cold methane T-dwarfs at distances ~ 200 pc, i.e. across the entire galactic disk. Objects with a mass of $\sim 0.01\ M_{\odot}$ can be observed up to a distance of 50 pc.

References

1. Kumar S S *Astrophys. J.* **137** 1121 (1963)
2. Salpeter E E *Astrophys. J.* **134** 669 (1961)
3. Chabrier G, Baraffe I *Annu. Rev. Astron. Astrophys.* **38** 337 (2000)
4. Jones H R A et al. *Mon. Not. R. Astron. Soc.* **267** 413 (1994)
5. Geballe T R et al. *Astrophys. J. Lett.* **467** L101 (1996)
6. Allard F "Model atmospheres for M-dwarfs", PhD Thesis (Heidelberg: Ruprecht-Karls Univ., 1990)
7. Miller S et al., in *Molecules in the Stellar Environment: Proc. of IAU Colloq. N 146, Copenhagen, Denmark, May 24 – 29, 1993* (Lecture Notes in Physics, Vol. 428, Ed. U G Jørgensen) (Berlin: Springer-Verlag, 1994)
8. Partridge H, Schwenke D W *J. Chem. Phys.* **106** 4618 (1997)
9. Allard F et al. *Annu. Rev. Astron. Astrophys.* **35** 137 (1997)
10. Rebolo R, Martin E L, Magazzu A *Astrophys. J. Lett.* **389** L83 (1992)
11. Pavlenko Y V et al. *Astron. Astrophys.* **303** 807 (1995)
12. Basri G, Marcy G W, Graham J R *Astrophys. J.* **458** 600 (1996)
13. Nakajima T et al. *Nature* **378** 463 (1995)
14. Martin E L et al. *Astron. Astrophys. Lett.* **327** L29 (1997)
15. Kirkpatrick J D et al. *Astrophys. J.* **519** 802 (1999)
16. Kenworthy M et al. *Astrophys. J. Lett.* **554** L67 (2001)

Additional reviews

1. Basri G "Observations of Brown Dwarfs" *Annu. Rev. Astron. Astrophys.* **38** 485 (2000)
2. *Brown Dwarfs and Extrasolar Planets: Proc. of a Workshop, Puerto de la Cruz, Tenerife, Spain, 17 – 21 March 1997* (Astron. Soc. of the Pacific Conf. Ser., Vol. 134, Eds R Rebolo, E L Martin, M R Zapatero Osorio) (San Francisco, Calif.: ASP, 1998)
3. *From Giant Planets to Cool Stars: Proc. of a Workshop, Northern Arizona Univ., Flagstaff, AZ, USA, 8 – 11 June 1999* (Astron. Soc. of the Pacific Conf. Ser., Vol. 212, Eds C A Griffith, M S Marley) (San Francisco, Calif.: ASP, 2000)

PACS number: **96.60.–j**

DOI: 10.1070/PU2002v045n08ABEH001194

Comprehensive solar studies by CORONAS-F satellite: new results

V N Oraevskiĭ, I I Sobel'man,
I A Zhitnik, V D Kuznetsov

1. The CORONAS program and CORONAS-F project

The paper presents the results of comprehensive studies of solar activity by the CORONAS-F satellite.

The launch of the near-Earth space solar observatory CORONAS-F was done within the framework of the international program CORONAS (Comprehensive Orbital Near-Earth Observations of Activity of Sun) which is devoted to studies of the Sun in different phases of the 11-year solar cycle. The previous satellite CORONAS-I (launched in 1994) observed the Sun near its activity minimum. The CORONAS-F will study the solar activity about the maximum of the current 23rd cycle. On July 31, 2001, the CORONAS-F satellite was launched into an orbit with the following parameters: orbital inclination 82.49°, minimal distance from the Earth surface 500.9 km, maximal distance from the Earth surface 548.5 km, and the orbital period 94.859 min. Such an orbit provides regularly repeating periods of continuous observations of the Sun with a duration of about 20 days, which is especially important for problems of helioseismology and solar spot patrolling. The stabilization of the spacecraft actually realized proved to be 3–5 times better than was projected (several arc seconds per second), which allows observations of the Sun with a high spatial resolution.

2. Scientific goals of the CORONAS-F project

The main scientific goals of the CORONAS-F project include observations of global solar oscillations and seismological studies of the solar interior, comprehensive studies of powerful dynamical process in the active Sun (active regions, flares, plasma ejecta) in a broad wavelength range from the optical to gamma-ray emission, studies of solar cosmic rays accelerated during active processes on the Sun, of their escape conditions, propagation in the interplanetary plasma, and their impact on the terrestrial magnetosphere.

3. Scientific payload and the first results of observations

In accordance with the scientific goals of the project, the scientific payload of the spacecraft includes four main groups of detectors: an instrument for registration of global oscillations of the Sun; X-ray spectral imaging detectors to study active regions on the Sun with a high spatial resolution of order of $2-3''$; detectors of electromagnetic fluxes from active regions and flares; and instruments for studies of corpuscular solar fluxes. The broad-band measurements of the electromagnetic spectrum and fluxes of both neutral (neutrons) and charged (electrons, protons, and nuclei) particles from the Sun allows the astronomers to obtain the most complete picture of physical processes underway in solar active regions. The CORONAS-F instruments and their main designation are listed in Table 1.

The scientific payload instruments (SPI) are basically operated from the Center of Flight Operation (CFO) of SPI at the Institute of Terrestrial Magnetism, Ionosphere and Radio Wave Propagation of RAS (IZMIRAN) at Troitsk, Moscow Region. The commands to the onboard SPI are issued every day. One batch of commands amounts to 24 Kb. In addition to the working regime operations, a dynamic on-flight re-programming is provided inside the onboard SPI controllers, which allows their software adjustment to current observations. The requirements to operation through the CFO IZMIRAN are collected via e-mail with a time interval not less than 10 minutes before the communication session, which provides the required operability and flexibility of the SPI control.

DIFOS spectrophotometer. The DIFOS spectrophotometer is designated to measure fluctuations of the optical emission intensity from the Sun with the aim of obtaining the spectrum of global solar oscillations. The intensity measurements are carried out simultaneously at six optical spectral bands: 350, 500, 650, 850, 1100, and 1500 nm with a 10% passband of the central frequency. In comparison with the CORONAS-I project, the photometer is largely upgraded: the sensitivity of photodetectors is significantly increased (by more than an order of magnitude), the spectral range of observations is enlarged by almost two times with a simultaneous increase in the number of channels from three to six. Observations of global solar oscillations are performed in the most informative line in the UV range in which the intensity of emission from global solar oscillations is appreciably larger than the intensity in other emission lines. Figure 1 compares the channels of the DIFOS detector with instruments onboard the SOHO satellite [1]. Of importance is that the DIFOS detector can make measurements in the short-wave channel at 350 nm — in the ultraviolet region where, according to some estimates, enhanced values of global oscillation amplitudes were expected. Equally important is that the device allows measurements over a wide spectral range from 350 nm to 1500 nm using one and the same method.

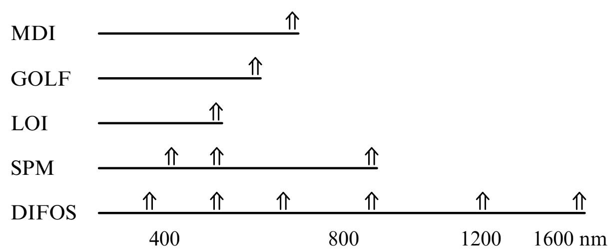

Figure 1. Comparison of channels of the DIFOS (CORONAS-F) spectrophotometer with the SOHO instruments (MDI — Michelson Doppler Imaging of Solar Oscillations, GOLF — Global Low-Degree Velocity, LOI — Luminosity Oscillation Imager, SPM – SunPhotoMeter).

Figure 2 shows the relative amplitudes of 5-minute oscillation modes of the Sun at the wavelength 350 nm over the period 28–30 November 2001 obtained by processing data taken by the DIFOS spectrophotometer. Similar spectra were obtained for all other channels. After averaging over modes, the mean values of the relative amplitudes were calculated for each of the six channels and their dependence on the wavelength was obtained. This dependence is shown in Fig. 3. All points lie along a smooth curve which is fitted by the law $\lambda^{-1.2}$. A similar result was obtained for the other observational period from November 30 to December 2, 2001 (the second curve on the figure marked with triangles). The DIFOS data show good agreement with the results obtained in the ground-based observation range [2]. According to the ground-based measurements, the amplitude ratio of the global oscillations at wavelengths 500 and 680 nm is 1.6, and the DIFOS data give 1.54. For another pair of wavelengths, 500 and 870 nm, the amplitude ratio is 2.2 in the ground-based observations and 1.93 according to the DIFOS data.

Spectral images of the full disk of the Sun in the X-ray range 1.85–335 Å (the SPIRIT experiment). The experiment SPIRIT includes the multi-channel telescope SRT-K and spectroheliograph RES-K. The main goal of the experiment is the simultaneous obtaining of X-ray spectral images of the solar disk and corona corresponding to mono-temperature

Table 1. Scientific payload of the CORONAS-F satellite.

Instrument	Designation	Institute where the instrument was designed	Scientific supervisors
		Helioseismology	
DIFOS spectrophotometer	Helioseismological monitoring	Institute of Terrestrial Magnetism, Ionosphere and Radio Wave Propagation of RAS (IZMIRAN)	V N Oraevskiĭ
		High angular resolution monochromatic imaging	
SRT-K solar X-ray telescope	Studies of spatial structure and dynamics of the upper solar atmosphere using narrow-band XUV-images	P N Lebedev Physics Institute of RAS	I I Sobel'man I A Zhitnik
RES-K X-ray spectroheliograph	Hot solar atmosphere plasma diagnostics by imaging in X- and XUV-spectral lines	P N Lebedev Physics Institute of RAS	I I Sobel'man I A Zhitnik
DIOGENESS spectrophotometer	X-ray studies of active regions on the Sun and solar flares	Space Research Center of the Polish Academy of Sciences	Ya Silwester
		Electromagnetic flux measurements (from UV to gamma-rays)	
RESIK X-ray spectrometer	X-ray solar studies with high spectral resolution	Space Research Center of the Polish Academy of Sciences	Ya Silwester
SPR-N solar spectropolarimeter	X-ray polarization studies of solar flares	P N Lebedev Physics Institute of RAS Institute of Nuclear Physics of MSU	I I Sobel'man I P Tindo S I Svertilov
IRIS flare spectrometer	X-ray studies of the solar flare activity	A F Ioffe Physical-Technical Institute of RAS	G E Kocharov
HELIKON gamma-ray spectrometer	X-ray and gamma-ray studies of solar flare activity	A F Ioffe Physical-Technical Institute of RAS	E P Mazets
RPS X-ray spectrometer	X-ray studies of solar flares and their precursors	Space Research Institute of RAS Moscow Engineering Physics Institute	V M Pankov Yu D Kotov
AVS amplitude-time spectrometer	X-ray and gamma-ray studies of solar flares	Moscow Engineering Physics Institute	Yu D Kotov
SUFR-Sp-K solar UV radiometer	Studies of the total UV flux variations from the Sun	E K Fedorov Institute of Applied Geophysics	T V Kazachevskaya
VUSS-L ultraviolet solar spectrophotometer	UV solar studies near the resonance hydrogen line H L_α	E K Fedorov Institute of Applied Geophysics	A A Nusinov
		Studies of corpuscular fluxes from the Sun	
SKL detectors for solar cosmic ray studies	Solar cosmic ray studies	Institute of Nuclear Physics of MSU	S N Kuznetsov
		Scientific data acquisition and processing	
System of scientific data acquisition (SSDA)	Operation by the scientific payload and its working regimes	Institute of Terrestrial Magnetism, Ionosphere and Radio Wave Propagation of RAS (IZMIRAN)	V N Oraevskiĭ A I Stepanov

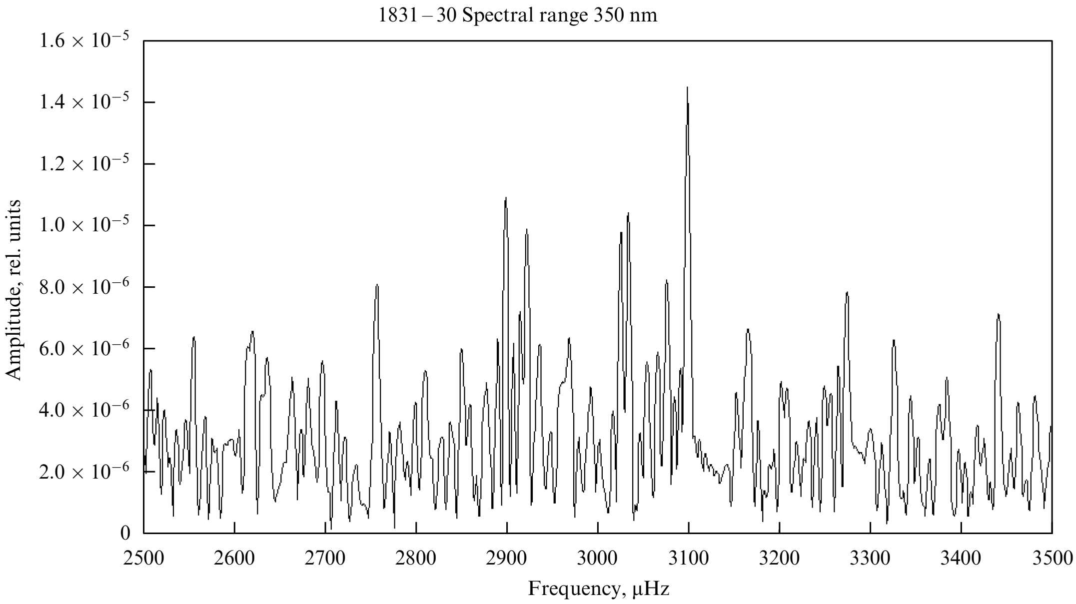

Figure 2. Relative amplitudes of the 5-min oscillation solar modes at the wavelength 350 nm obtained by the DIFOS spectrophotometer.

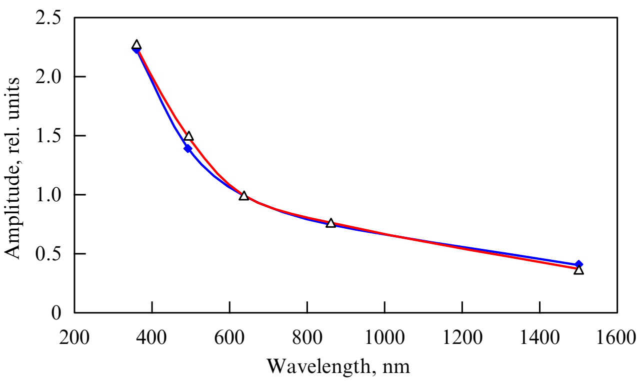

Figure 3. Relative amplitude of global solar oscillation as a function of the observation wavelength.

Table 2. Principal characteristics of the measurement channels of the SRT-K and RES-K instruments.

Channel range, Å	Main ions	T, 10^6 K
1.85 – 1.87	FeXXIV – XXV	20 – 50
8.418 – 8.423	MgXII	10
177 – 207	OIV, FeIX – XXIV, CaXIV – XVII	0.3 – 16
285 – 335	HeII, SiXI, FeXV – XVI, MgVIII, NiXVII, CaXVII	0.05 – 5
171	FeIX – X	1.3
175	FeX – XI	1.3
195	FeXII	1.6
284	FeXV	2
304	HeII	0.05
304	HeII, FeXV	0.05 – 2

plasma layers of the solar atmosphere over a wide temperature range $T_e = 0.05-50$ MK (1 MK $= 10^6$ K) with a high spatial, spectral, and time resolution. These observations of the Sun are basic for studies of the three-dimensional structure and dynamics of the solar atmosphere, for the determination of physical parameters and variations of element abundance in plasma structures and phenomena, such as active regions, coronal holes, flares, coronal mass ejections, bright points, prominences, etc.

The SRT-K and RES-K instruments include multi-layer focusing optics, systems of thin-film and porous spectral filters, and detectors based on open microchannel plates and cooled CCD-matrices. An important feature of the devices is the possibility of simultaneous imaging of the entire Sun in several spectral channels. (A detailed description and schemes of the instruments can be found in Ref. [3].) The main characteristics of the measurement channels are collected in Table 2. Narrow-band channels centered on the wavelengths 171, 175, 195, 284, and 304 Å relate to the SRT-K telescope; other channels belong to the RES-K spectroheliograph. The MgXII channel yields monochromatic images in the line 8.42 Å with an angular resolution of $6'' \times 6''$. Spectroheliograms recorded at wavelengths 177 – 207 Å and 285 – 335 Å provide simultaneous spectra of plasma structures in the solar atmosphere with a spatial, spectral, and time resolution of $5'' \times 100''$ and $8'' \times 160''$, 0.02 and 0.04 Å, and up to 2 s, respectively.

Over the first year of observations, more than 100 thousand X-ray images and spectroheliograms were taken in the wavelength range 8.4 – 335 Å with a high spatial, spectral, and time resolution. More than 200 images of the Sun are registered every day. As an example, Figure 4 shows images of the Sun taken in the X-ray telescope channels which correspond to temperature layers in the range 0.05 – 2 MK (see Table 2). Local and large-scale plasma structures, various magnetic field configurations, as well as a flare region are visible on the images. Figure 5 shows the monochromatic image in the line MgXII 8.42 Å of a solar corona region heated up to a temperature of 10 MK. This image is superimposed with a snapshot taken in the 175 Å channel corresponding to the temperature of 1.3 MK (the spherical structure in the upper right corner in Fig. 5). The high-

X-ray solar images by the SRT-K telescope

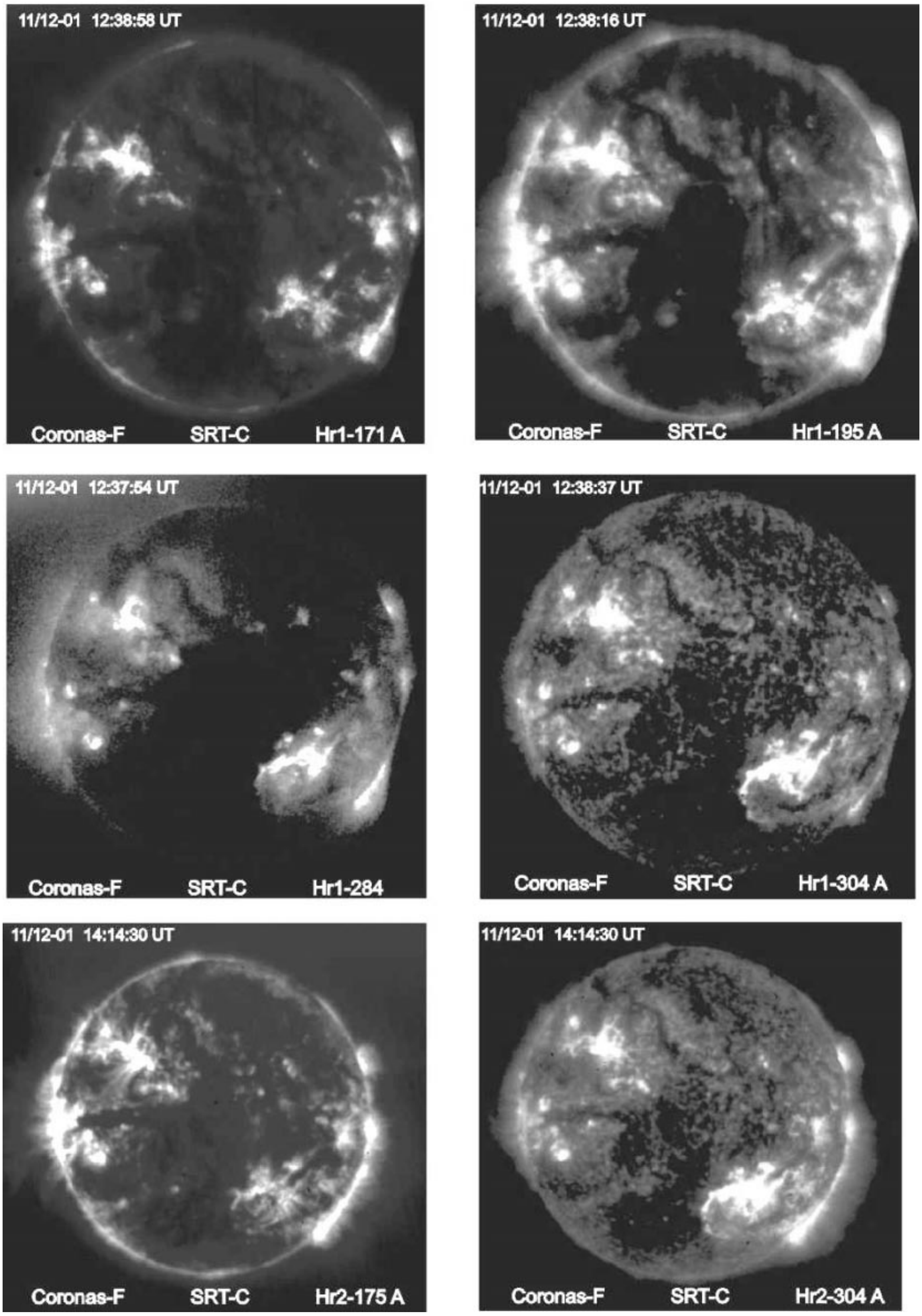

Figure 4. Solar images taken in the channels of the X-ray telescope corresponding to temperature layers in the range 0.05 – 2 MK (the SPIRIT experiment).

temperature (10 MK) dynamical plasma structures with different life times (from minutes to tens hours), of various forms (helmet-like, spherical, spider-like, etc.) and with different height distributions up to a hundred thousand km above the solar disk have been discovered on the monochromatic X-ray images for the first time.

Figure 6 shows the spectroheliogram of the Sun of 16.09.01, 03:59 UT together with the flare spectrum in the range 177 – 207 Å. This spectrum also exhibits principal intensive lines of the FeX – FeXXIV ions excited in a wide temperature range from 1 to 16 MK, as well as some lines of ions of other elements (O, Ca, and Ni) corresponding to

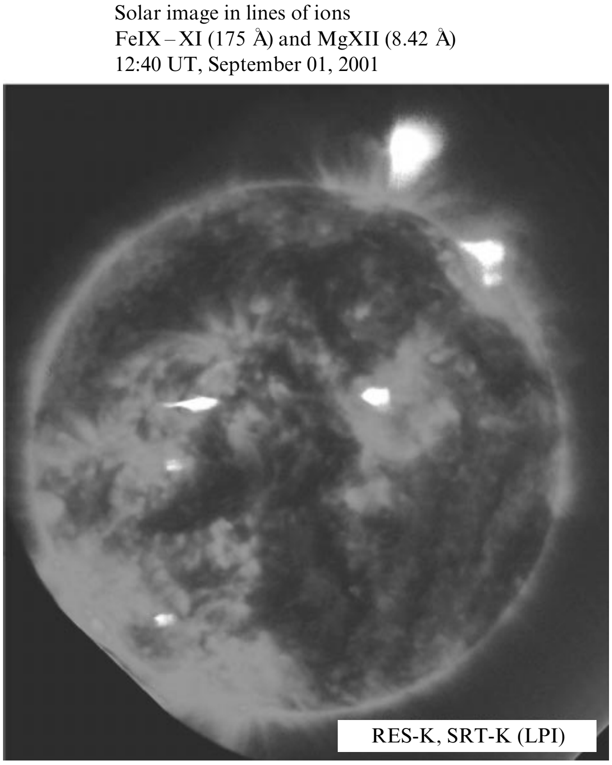

Figure 5. Monochromatic solar image in the line MgXII 8.42 Å of the solar corona region heated up to a temperature of 10 MK [the SPIRIT experiment, P N Lebedev Physics Institute of RAS (LPI)].

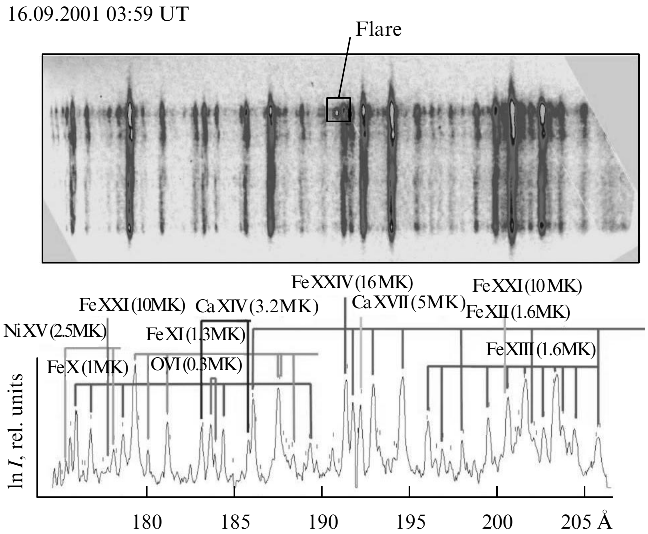

Figure 6. Spectroheliogram of the Sun of 16.09.01 (03:59 UT) together with the spectrum of a flare in the range 177 – 207 Å. Also shown are the principal strong lines of ions FeX – XXIV excited in the wide temperature range from 1 to 16 MK, as well as some lines of other element ions (O, Ca, and Ni) corresponding to temperatures 0.3 – 5 MK (the SPIRIT experiment).

temperatures 0.3 – 5 MK. The flare region appears as a compact image on the spectroheliogram in the 'hot' line FeXXIV 192.04 Å which has a maximum at 16 MK.

A preliminary analysis of images in the emission lines of multicharged ions yielded electron density and temperature distributions in different plasma formations of the solar

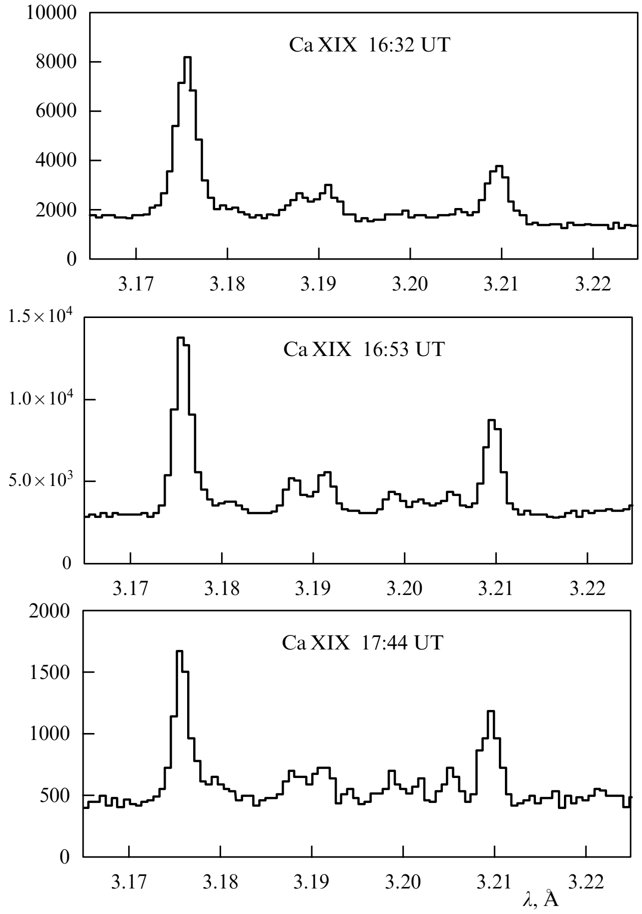

Figure 7. Spectra in the line CaXIX with a high spatial resolution ($\sim 5''$) on the increasing phase, the intermediate phase, and the decay phase of the most powerful flare of the current solar activity cycle (August 25, 2001, the DIOGENESS spectrophotometer).

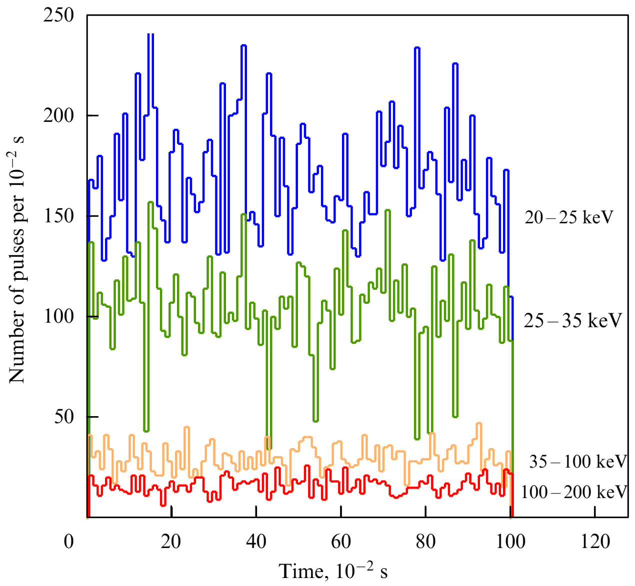

Figure 8. Record of the hard X-ray intensity emission in four energy channels in the range 20 – 100 keV with a high time resolution for the event of September 27, 2001, 18:26 UT (the IRIS flare spectrometer).

corona: active regions, flares, coronal holes, etc., lying in the range $N_e \approx 10^8 - 10^{12}$ cm^{-3} and $T_e \approx 1 - 20$ MK.

Thus, within the framework of the SPIRIT experiment, a novel field in solar astrophysics, X-ray imaging spectroscopy, has been elaborated, which allows the astrophysicists to reconstruct from monochromatic images of the Sun its three-dimensional structure and to study dynamics of plasma formations in the solar atmosphere in the temperature range $T_e \approx 0.05 - 50$ MK.

The DIOGENESS spectrophotometer and the RESIK X-ray spectrometer. The RESIK and DIOGENESS instruments measure solar emission spectra in the wavelength range 3 – 7 Å and are designated for X-ray studies of active regions and flares with a high spectral resolution. The X-ray solar emission spectra obtained by these detectors are comparable by spectral and time resolution with the best observations available so far. The polar orbit of the CORONAS-F satellite, as well as the complete coverage of a wide spectral range, make these spectra a valuable addition to those obtained by the Yohkoh satellite. At large X-ray fluxes, the detectors of the RESIK device and Yohkoh spectrophotometers saturate, so DIOGENESS is at present the only working spectrometer worldwide which takes spectra of the powerful flares of importance above M2 (an example is provided by the flare of X5.3 class of August 25, 2001).

Figure 7 displays spectra taken in the line CaXIX with a high spatial resolution ($\sim 5''$) at the growing phase, intermediate phase, and decay phase of the most powerful flare of the current solar activity cycle (of August 25, 2001). The emitting plasma temperature decreases from 2.5 MK at the growing phase to 1.2 MK at the decay phase. The spectral line width changes are clearly visible on the spectra, which is indicative of the important role of plasma turbulence during the flare evolution. The relative line intensities contain information on the energy balance in the flares, and the role of non-Maxwell and non-equilibrium processes in the energy

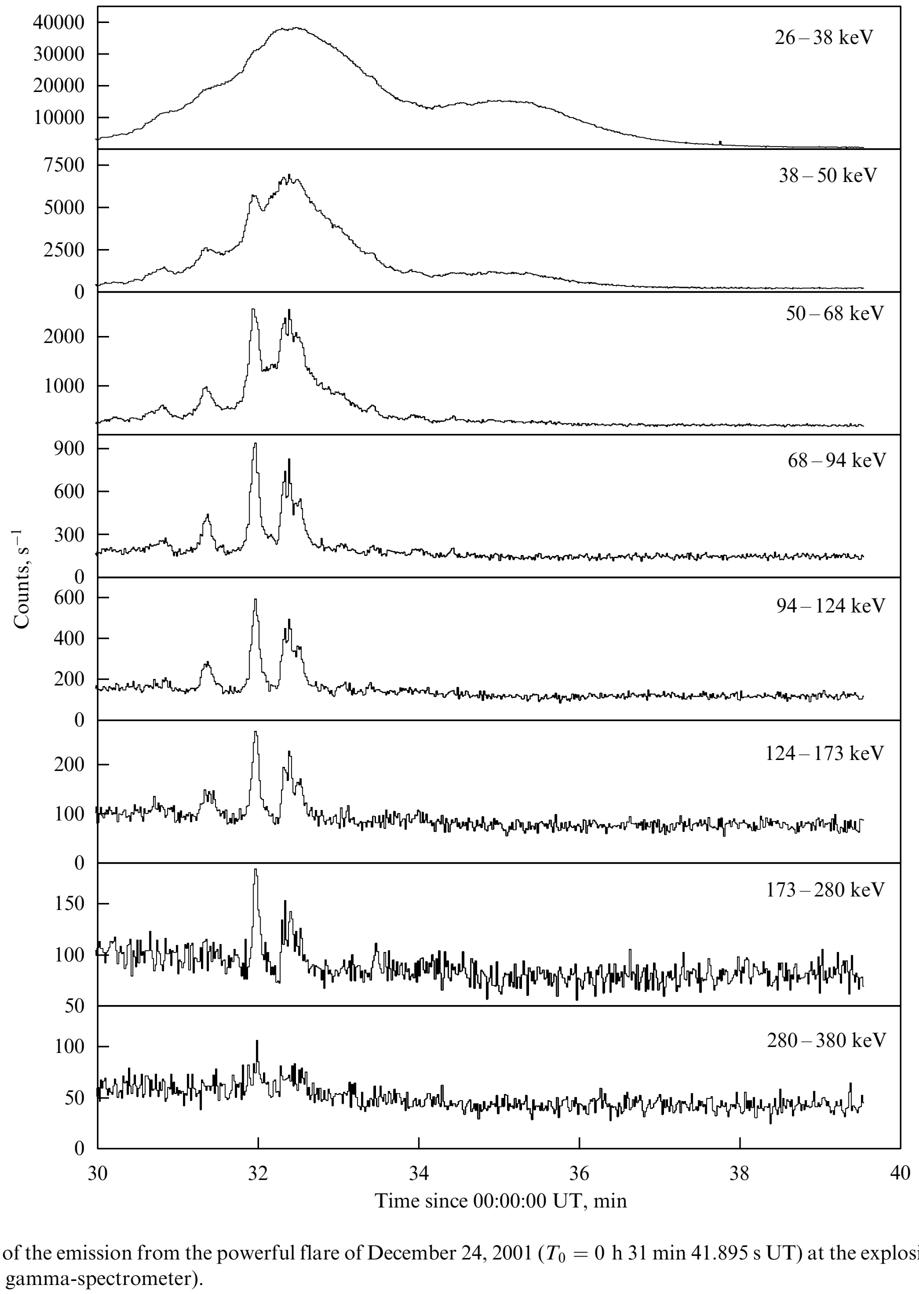

Figure 9. Time profile of the emission from the powerful flare of December 24, 2001 ($T_0 = 0$ h 31 min 41.895 s UT) at the explosion phase in eight energy channels (HELIKON gamma-spectrometer).

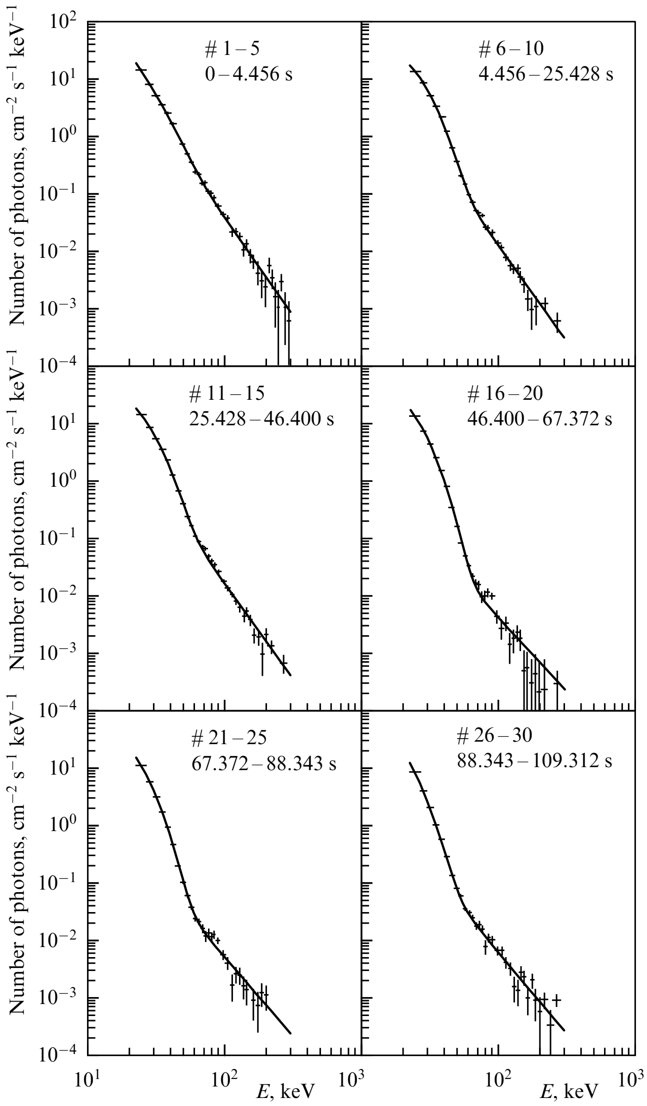

Figure 10. Energy spectra of the powerful flare of December 24, 2001 taken successively at different phases of the event (0 – 109 s) (HELIKON gamma-spectrometer).

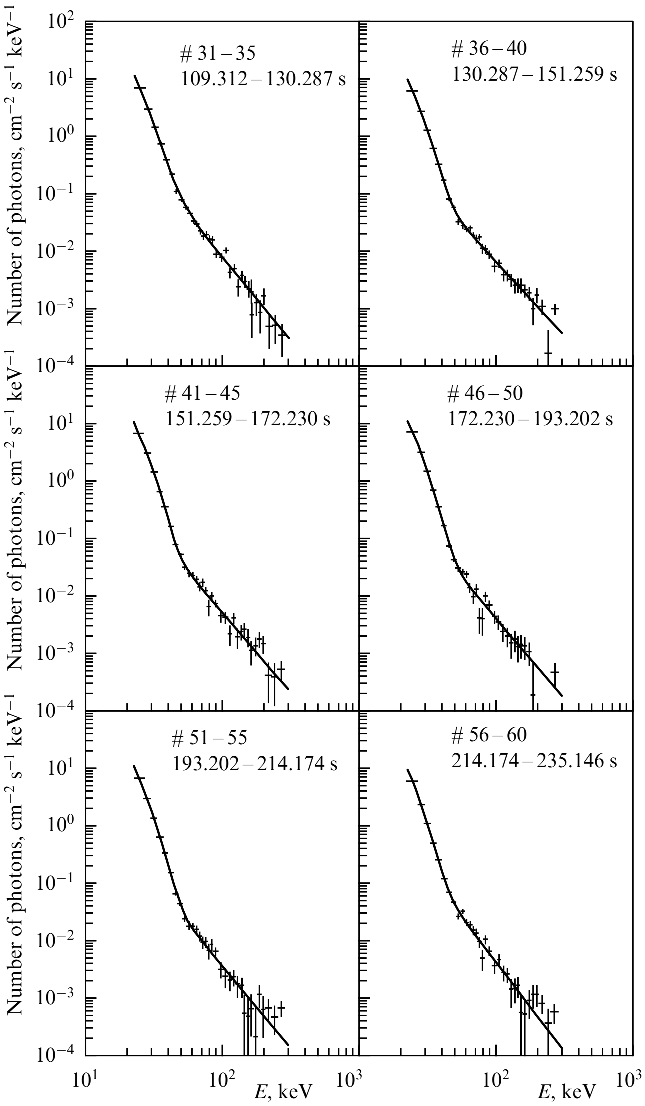

Figure 11. Energy spectra of the powerful flare of December 24, 2001 taken successively at different phases of the event (109 – 235 s) (HELIKON gamma-spectrometer).

release region of the flare. In this spectral range (3 – 7 Å), such high-resolution spectra of an X-class flare have been obtained for the first time. They demonstrate the presence of many emission lines which are produced by collisional excitation of atoms, by excitation of internal atomic shells and dielectronic recombination, and provide a detailed diagnostics of the flare plasma.

The IRIS flare spectrometer. The instrument is designated for the solar flare activity studies in the X-ray range 2 – 200 keV. In the patrol regime, it has 12 energy channels with a time resolution of 2.5 s; in the flare regime — 64 energy channels with a time resolution of 1 s and 4 channels with a resolution of 10 ms. Thus far no spectral measurements with such a high time resolution have been obtained in X-ray solar experiments. The fine time structure observations of X-ray flux provide direct information on the development of the energy release processes at the flare explosion phase and allow us to advance in understanding their physical mechanism. Figure 8 presents the records of the hard X-ray emission in 4 energy channels in the range 20 – 100 keV with a high time resolution for the event of September 27, 2001, 18:26 UT.

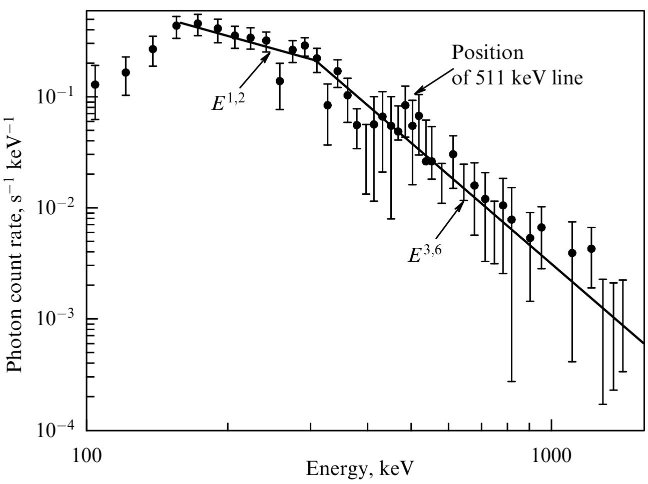

Figure 12. Differential energy spectrum of the event of 18.09.2001 obtained with the AVS amplitude-time spectrometer.

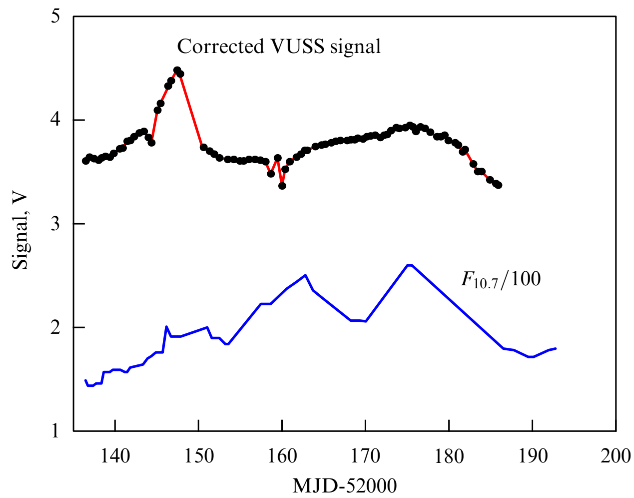

Figure 13. VUSS-L time record of the signal proportional to the UV flux and the solar radio emission flux at the wavelength of 10.7 cm. Along the x-axis are days in MJD. \

The HELICON gamma-spectrometer. This instrument registers time and spatial characteristics of hard electromagnetic radiation from solar flares in a wide energy range from X-ray to gamma-ray (10 keV – 10 MeV). Using this device, observation of a radiation situation in near-Earth space and soft-energy solar flares is being carried out. It also allows the registration of hard ($E_\gamma > 50$ keV) flares and gamma-ray bursts. Over the observation period from August 15, 2001, to January 22, 2002, the HELICON detector registered more than 600 solar flares and 5 gamma-ray bursts. Most flares had soft spectra and were detected in the background regime with a time resolution of 1 s in eight consecutive energy intervals from 26 to 380 keV. One of the powerful solar flares was registered at the explosion phase on 24 December at $T_0 = 0{:}31{:}41.895$ UT. Figures 9 – 11 show the temporal dynamics of this flare in the eight energy channels and the energy spectra taken successively at different phases of the event. The starting time of registration of each spectra and the duration of data acquisition are also shown in the figures.

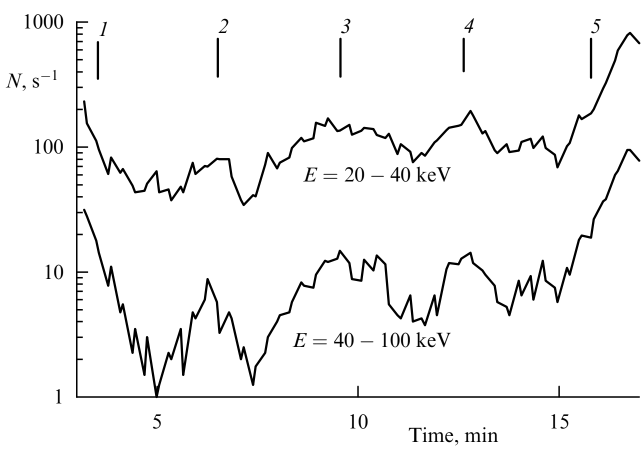

Figure 14. The record from the X-ray monitoring detector SPR-N taken during a solar flare. The increases *1*, *2*, and *5* are the bremsstrahlung radiation from magnetosphere electrons. The increases *3* and *4* correspond to the X-ray emission from the source outside the magnetosphere (the solar flare).

The RPS-1 X-ray spectrometer. The instrument is designated to study solar flares and their precursors in the X-ray range 3 – 30 keV. Over the time of observations, calibration characteristics of the instrument were corrected, background maps were obtained, and experimental data statistics were acquired. No observations have been carried out by SOHO satellite in this energy range and the results of the SXS experiment onboard the Yohkoh satellite have not been published as yet.

The AVS amplitude-time spectrometer. This instrument is designated for X-ray and gamma-ray studies of solar flares, and in particular, for analysis of the events like a 'solar-flare — gamma-ray burst' within the energy ranges $E = 3$ – 30 keV, $E = 0.1 - 8.0$ MeV, and $E = 2.0 - 80.0$ MeV. Over the observation time, several tens of candidate events like a 'solar flare – gamma-ray burst' have been detected. For these events energy spectra are obtained at different phases of the event (before, during, and after the event). The duration of the candidate events varies from 16 s to 3 – 5 min. Figure 12 presents the measured differential energy spectrum for the event of 18.09.2001, on which a break at the energy 300 keV and a spectral feature which can be related to the 511 keV annihilation line are visible.

The SUFR-Sp-K solar ultraviolet radiometer. The SUFR-Sp-K detector measures ultraviolet radiation flux from the Sun as a star in several spectral intervals from 1 to 130 nm, which comprises, in contrast to the SOHO satellite, a *wider* spectral range. Aside from scientific goals, the detector performs monitoring of one of the most essential element of space *weather*, the geoeffective solar radiation. Using the SUFR instrument, X-ray data on the powerful X-5.3B solar flare which occurred on August 25, 2001, 16 h 23 min UT, was obtained at $\lambda < 12$ nm.

VUSS-L ultraviolet solar spectrophotometer. The VUSS-L instrument measures radiation at the wavelength 120 nm and is designated to study the UV solar radiation near the resonance hydrogen line H L_α. Extensive measurements of the ultraviolet radiation flux in the Lyman-alpha line with a preliminary estimated intensity of ~ 10 erg cm^{-2} s^{-1} have been carried out by this detector. A time record from the VUSS-L detector is reproduced in Fig. 13.

The UV radiation from the Sun as a star registered by the SUFR-Sp-K and VUSS-L instruments has an impact on the upper layers of the Earth's atmosphere and is an important characteristic of the solar activity over its cycle.

The complex of detectors SCR for solar cosmic ray studies. The scientific payload SCR includes three instruments: SONG (Spectrometer of gamma-ray emission and neutrons, supervised by S P Ryumin), MCL (Cosmic ray monitor, supervised by S N Kuznetsov), SCI-3 (Spectrometer of cosmic radiation, supervised by A F Podorol'skiĭ). It is designated for comprehensive studies of solar cosmic rays and their manifestations in near-Earth space. The SONG detector registers X-ray and gamma-ray spectra in the energy range 0.03 – 100 MeV, spectra of gamma-ray lines in the range 0.3 – 20 MeV, neutrons with energy > 20 MeV, fluxes of cosmic ray particles — protons with energy > 70 MeV and electrons with energy > 50 MeV. The MCL detector measures fluxes and spectra of protons with energy 1 – 200 MeV and electrons with energy 0.5 – 12 MeV. The SCI-3 instrument measures the chemical composition and spectra of ions with $Z = 1 - 10$ in the energy range 1.5 – 20 MeV per nucleon for He, 4 – 40 MeV per nucleon for Ne. Compared to instruments onboard the SOHO and Yohkoh satellites, the

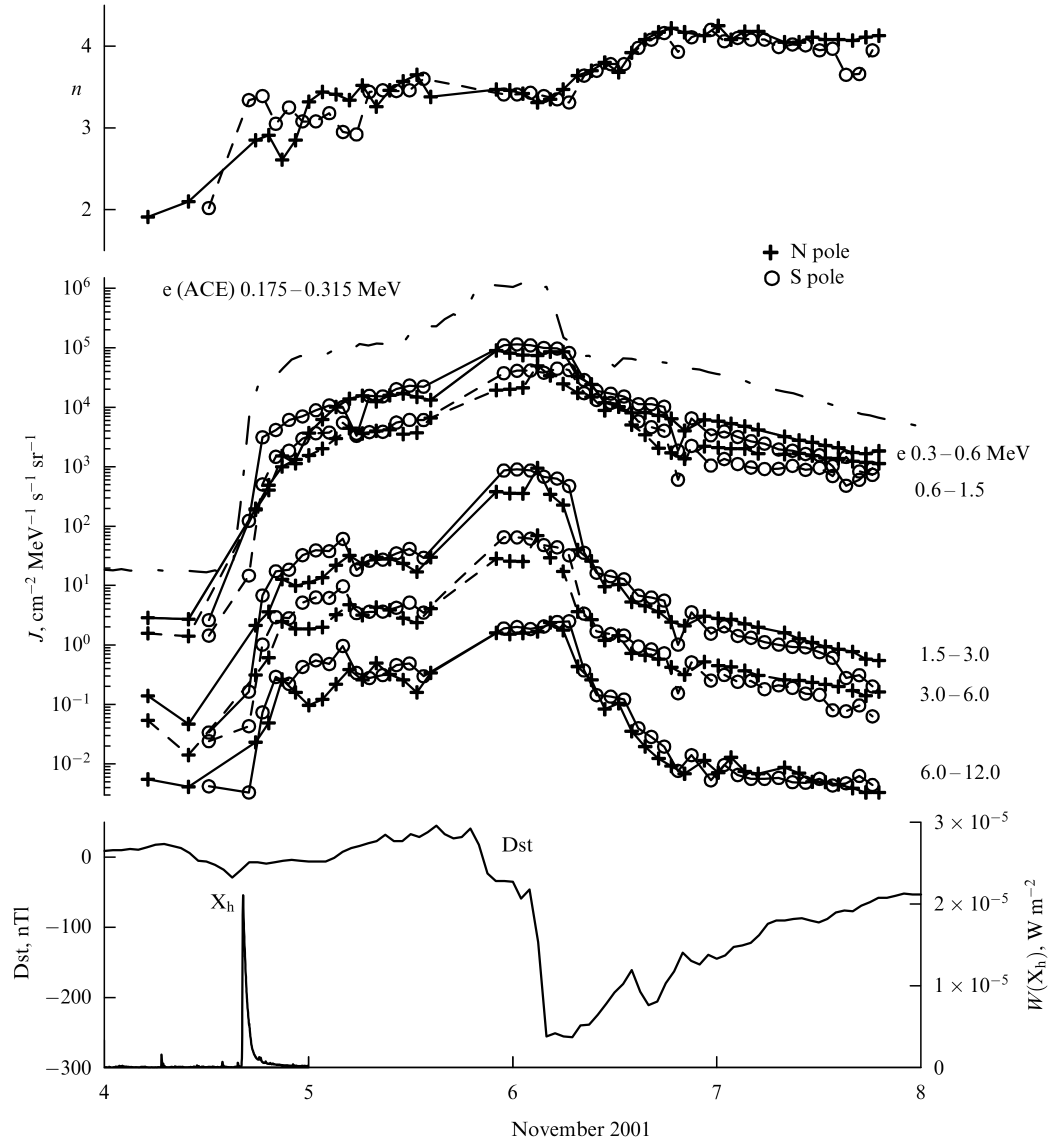

Figure 15. Some consequences of the solar flare of November 4, 2001, in interplanetary space and the Earth magnetosphere. The bottom panel: X_h — thermal X-ray emission of the flare according to the GOES 8 data, the Dst-variation on November 4 – 7, 2001. The middle panel — the electron fluxes with energy 0.175 – 0.315 MeV in interplanetary space (the ACE satellite data), as well as the electron fluxes with energy 0.3 – 12 MeV in the polar caps (the SCR CORONAS-F complex). The upper panel shows the variation of the electron energy power-law index with time (the SCR CORONAS-F complex).

SONG spectrometer is capable of detecting high energy gamma-quanta (up to 100 MeV), which, in turn, makes it possible to observe gamma-quanta from decays of π^0-mesons that form by high energy proton interactions. The results obtained by the CORONAS-F satellite demonstrated that the background noise of the SONG instrument in the measurements of solar neutrons is 5 – 7 times lower than of the GRS (SMM) — the only detector that measured solar neutrons in the same energy range.

The flare of 04.11.2001 at 16 h 20 min UT initiated one of the largest increases of the solar particle flux in near-Earth space. Figure 14 shows data from the patrol detector of the SPR-N device. During these observations, the satellite crossed the polar cap. The X-ray flux in the intervals *1* and *5* corresponds to the bremsstrahlung radiation of the external belt electrons; in region *2*, a burst of magnetospheric electrons was observed (data from the MCL detector); regions *3* and *4* correspond to a real X-ray emission increase. A comparison with the GOES satellite data showed that in spite of continuous growth of the thermal X-ray emission flux from 16 h 03 min to 16 h 20 min UT, the bremsstrahlung radiation indicated at least two pulses of particle acceleration on the Sun.

After the flare, high energy solar particles appeared and on November 5 at 20 h UT geomagnetic perturbations started, connected with the arrival of the coronal plasma ejected in the November 4 flare. The bottom panel of Fig. 15 shows the emission from the solar flare at 16:20 UT on November 4 according to the GOES 8 data, and the Dst-variation. It is seen that the geomagnetic perturbation due to the arrival of the coronal mass ejection (CME) started at around 20 h UT on November 5. The mean CME propagation velocity is $\sim$ 1700 km s^{-1}, so a strong shock wave must form ahead of the CME. Measurements of the interplanetary magnetic field strength by the ACE, WIND and GEOTAIL satellites confirm this conclusion. This shock wave can be a powerful source of high-energy particles. Measurements of protons and ions with energy from 1 to 100 MeV per nucleon

Table 3. Percentage abundance of different elements (nuclei with energy 11.4 – 23 MeV per nucleon) relative to oxygen for four time intervals during the flare of November 4 – 7, 2001.

Time	C	N	O	Ne	Mg	Si
22 h 04 Nov – 15 h 05 Nov	39.0 ± 3.9	11.9 ± 1.7	100	14.4 ± 2.3	17.9 ± 2.4	17.4 ± 2.2
22 h 05 Nov – 07 h 06 Nov	45.5 ± 3.4	10.4 ± 1.3	100	12.0 ± 1.4	20.6 ± 2.0	16.8 ± 1.9
07 h 06 Nov – 19 h 06 Nov	42.4 ± 6.5	11.2 ± 2.7	100	12.4 ± 2.7	16.8 ± 3.4	10.4 ± 2.6
19 h 06 Nov – 20 h 07 Nov	54.7 ± 12.6	8.5 ± 2.0	100	12.2 ± 4.6	21.6 ± 6.7	18.9 ± 6.0

indicated an increase in these particle fluxes from the moment of the flare to the CME arrival at the Earth. The shock wave effectively accelerated electrons. The middle panel of Fig. 15 displays the time dependences of the electron fluxes with energy from 0.3 to 12 MeV, which have not been measured by other satellites in this time outside the geomagnetosphere. The upper panel of Fig. 15 shows the electron energy power-law index variations. The electron energy spectrum did not vary significantly as the CME approached the Earth. The electron spectra became softer, and the electron, as well as proton and ion, fluxes started decreasing as the CME receded from the Earth.

The CORONAS-F satellite also measured the ion fluxes with energy from 2 to 40 MeV per nucleon. The time variations of ions from C to Si were similar to proton and electron variations. The chemical composition of ion fluxes over the entire duration of the high-energy particle outburst practically did not change. Table 3 shows the percentage abundance of different elements relative to oxygen for the flare of November 4 – 7, 2001.

Acknowledgments. The authors thank T V Kazachevskaya, Yu D Kotov, G E Kocharov, S N Kuznetsov, N I Lebedev, E P Mazets, A A Nusinov, V M Pankov, A F Podorol'skiĭ, S P Ryumin, and Ya Silwester for providing the processed data from the CORONAS-F satellite, which were used in writing the present paper.

References

1. *The SOHO Mission: Scientific and Technical Aspects of the Instruments* (ESA SP, 0379-6566, № 1104, Compiled by T D Guyenne) (Paris: European Space Agency, 1989)
2. Jimenez A et al. *Astron. Astrophys.* **193** 298 (1988)
3. Avetisyan E A et al. "Rentgenovskaya izobrazhayushchaya spektroskopiya Solntsa v oblasti 1.85 – 335 Å v eksperimente SPIRIT (SRT-K, RES-K) na sputnike KORONAS-F" (X-ray imaging spectroscopy of the Sun at 1.85 – 335 Å in the SPIRIT (SRT-K, RES-K) experiment onboard the CORONAS-F satellite) *Pis'ma Astron. Zh.* (in press)

PACS numbers: 04.40.Dy, **97.60.–s**

DOI: 10.1070/PU2002v045n08ABEH001193

Wolf – Rayet stars and relativistic objects

A M Cherepashchuk

1. Introduction

Wolf – Rayet (WR) stars, identified by strong broad emission lines of helium, nitrogen, carbon, and oxygen at different ionization states, were discovered by French astronomers M Wolf and G Rayet in 1867 [1]. We shall consider only massive ($m = 5 - 50 M_\odot$) WR stars of the galactic type I population, which concentrate on average towards the galactic plane. Low-mass hot stars observed as nuclei of planetary nebulae also exhibit WR signatures; we shall not consider them in the present paper.

In total, 227 WR stars are known in our Galaxy and about 300 in nearby galaxies [2]. The full number of WR stars in the Galaxy is estimated to be one – two thousand.

Recently, a close relation between WR star evolution and the formation of neutron stars (NS) and black holes (BH) [3 – 5], as well as cosmic gamma-ray burst generation [6, 7], has been revealed.

2. On the nature of WR stars

According to modern concepts, WR stars are the naked helium cores of originally massive ($m > 30 - 40\ M_\odot$) stars that lost most of their hydrogen envelopes either as a result of mass exchange in close binary systems (CBS) [8], or due to intensive mass outflow from single stars in the form of stellar wind [9, 10]. The powerful emission line spectrum of WR stars forms at the base of stellar wind moving with velocities of 1 – 3 thousand km s^{-1} apparently due to radiation pressure from the hot 'core' at a rate of $\sim 10^{-5} M_\odot$ per year (see monographs [11, 12] and references therein). The mechanism of the WR wind acceleration has not yet been finally established.

WR stars are subdivided into two sequences: the nitrogen one (WN) and the carbon one (WC). The spectra of WN stars are mainly dominated by nitrogen lines, while WC spectra mostly show the presence of carbon and oxygen. Besides, among WR stars a small group of stars with enhanced oxygen lines (WO-stars) can be separated.

The spectra of WN and WC stars show both helium and hydrogen lines, however the hydrogen lines are very weak due to the predominantly helium chemical composition of WR stars. The sequence WN – WC – WO is interpreted as an evolutionary one [8]. Immediately after the massive star core exposure, it is enriched by products of the CNO-cycle of thermonuclear reactions. So initially the surface of the WR-star is enriched with nitrogen (the WN-stage). As the star loses mass via stellar wind, the layers enriched with carbon due to thermonuclear conversion of helium in triple α-particle collisions are exposed (the WC-stage). The subsequent mass loss exposes the WR star layers enriched with oxygen due to the reaction of α-particle captures by carbon atoms (the WO-stage). The mean mass of the WN stars is $\sim 22\ M_\odot$ and of the WC stars is $12\ M_\odot$, which is qualitatively consistent with the described evolutionary scenario for WR stars. About half of WR stars occur in binary systems WR + O which contain massive hot stars of spectral class O as companions.

WR stars, as massive, hot, non-degenerate, mainly helium stars at late evolutionary stages, must explode as type Ib or type Ic supernovae and form relativistic objects as a result of the collapse of their CO-cores. Besides, the absence of